Supporting Information

Experimental methods

1. Chemicals

All chemicals were used without further purification unless otherwise stated. Ethanol (≥99.7%) and methyl alcohol (≥99.5%) were purchased from Chengdu Organic Chemicals Co., China. Nafion solution (5 wt.%) was purchased from Sigma-Aldrich. 2 methylimidazole ($C_4H_6N_2$, 98%), iron(III) nitrate heptahydrate ($Fe(NO_3)_3·9H_2O$, ≥99%), sulfuric acid (H_2SO_4, 96%), zinc nitrate hexahydrate ($Zn(NO_3)_2·6H_2O$, ≥99%), nickel(II) nitrate hexahydrate ($Ni(NO_3)_2·6H_2O$, ≥99%), and urea ($(NH_2)_2CO$, ≥99%), ammonium fluoride (NH_4F; AR, 96%) were purchased from Sigma-Aldrich. Acrylic acid was bought from Alfa Aesar. High-purity oxygen (O_2, 99.999%+) gas and high-purity argon (Ar, 99.999%+) were obtained from Kunming Hongfa Gas Products Co. Ltd. Deionized water was prepared by laboratory water purification system (HHitech Master-S30UVF) with a resistivity of 18.2 MΩ·cm (at 25 °C). Pt/C (20 wt.%, Alfa Aesar) and Ir/C (20 wt.% of Ir, Premetek Co.) were used as the benchmarks for oxygen reduction reaction (ORR) and oxygen evolution reaction (OER), respectively.

2. Material characterization

The obtained materials were characterized using scanning electron microscopy (SEM, Nova Nano SEM 430, operated at 10 kV), transmission electron microscopy (Tecnai F20, 200 kV; Titan Cubed Themis G2, 300 kV), X-ray photoelectron spectroscopy (XPS, Escalab 250, Al Kα), inductively coupled plasma mass spectrometry (ICP-MS, Perkin Elmer Optima 4300 DV), Raman spectroscopy (Jobin

Yvon HR800), and X-ray diffraction (XRD, Rigaku Miniflex 600, 40 kV). The specific surface area and pore structure of the samples were investigated with an automatic volumetric sorption analyzer (Autorsorb-IQ-3MP) using N_2 as the adsorbate at -196 °C.

X-ray absorption spectroscopy measurement at Fe K-edge was performed at the Advanced Photon Source on the bending-magnet beamline 9-BM-B with electron energy of 7 GeV and average current of 100 mA. The radiation was monochromatized by a Si (111) double-crystal monochromator. Harmomic rejection was accomplished with Harmonic rejection mirror. All spectra were collected in fluorescence mode by vortex four-element silicon drift detector. XAS data reduction and analysis were processed by Athena software.

3. Electrochemical measurements

Electrochemical measurements were performed on an electrochemical analysis station (CHI 700 E, 760 E and 1130 E, CH Instruments, China) using a standard three-electrode cell. A graphite rod and an Ag/AgCl electrode in a saturated KCl solution served as the counter electrode and reference electrode, respectively. All potential values refer to that of a reversible hydrogen electrode (RHE). To prepare the working electrode, 5.0 mg of each catalyst was ultrasonically dispersed in ethanol containing 0.05 wt.% Nafion (1.0 ml) to form a concentration of 5.0 mg ml^{-1} catalyst ink. The catalyst ink was then coated on the surface of the glassy carbon disk for the RRDE and RDE tests. The noble-metal-free catalyst loading was 0.6 mg cm^{-2}. Commercial Pt/C (20 wt.%, Alfa Aesar) and Ir/C (20 wt.% of Ir, Premetek Co.) catalysts with a standard

loading of 0.2 mg cm^{-2} were respectively used as ORR and OER reference samples. The linear scan voltammogram (LSV) curves in this work were corrected with *iR* compensation.

For the RRDE tests, the polarization curves were collected at disk rotation rates of 1600 rpm. The scan rate was 5 mV s^{-1} and the potential of ring was set at 0.3 V (vs. Ag/AgCl). The collecting efficiency of the RRDE (N) was 0.37. The peroxide yield (HO_2^-%) and the electron transfer number (n) was calculated as follows:

$$HO_2^- \% = 200 \times \frac{I_r/N}{I_d + I_r/N}$$

$$n = 4 \times \frac{I_d}{I_d + I_r/N}$$

where I_d is the disk current and I_r is the ring current. The ORR durability was evaluated by testing the LSV of NiFe&FeNCL/G modified electrode at 1600 rpm before and after 5000 continuous cyclic voltammetry (CV) potential cycles.

The RDE polarization curves for OER were collected in 0.1 M KOH solution at a disk rotation rate of 1600 rpm. The scan rate was 5 mV s^{-1}. The OER durability was evaluated by testing the LSV of NiFe&FeNCL/G modified electrode at 1600 rpm before and after 5000 continuous CV potential cycles.

The kinetic current density was derived from mass transport correction on the basis of the Koutechy-Levich formula:

$$\frac{1}{j} = \frac{1}{j_k} + \frac{1}{j_L} = \frac{1}{B\omega^{\frac{1}{2}}} + \frac{1}{j_k}$$

$$B = 0.2nFC_0 D_{O_2}^{\frac{2}{3}} v^{\frac{1}{6}}$$

$$j_k = nFkC_0$$

where j is the measured current density, j_k is the kinetic current density, j_L is the diffusion-limiting current density, ω is the rotating electrode angular velocity, F is the Faraday constant (F = 96,485 C mol^{-1}), C_0 is the bulk concentration of O_2 in the electrolyte ($C_0 = 1.26 \times 10^{-6}$ mol cm^{-3}), D_0 is the diffusion coefficient of O_2 in the electrolyte ($D_0 = 1.93 \times 10^{-5}$ cm^2 s^{-1}), ν is the kinematic viscosity of the electrolyte ($\nu = 1.009 \times 10^{-2}$ cm^2 s^{-1}), and k is the electron-transfer rate constant.

Turn-over frequency (TOF, number of electrons reduced per Fe-N_4 active site and per second at 0.9 V) of FeNCL/G for ORR was calculated according to the following formula:

$$TOF_{Fe-N4} = \frac{j_k}{\frac{W_{Fe-N4}}{M_{Fe}} \times N_A \times m_{loading}}$$

$$= \frac{3.45\ (mA \cdot cm^{-2}) \times 10^{-3} (A \cdot mA^{-1})}{\frac{1.95 \times 10^{-2} (wt.\%)}{55.85 (g \cdot mol^{-1})} \times 6.02 \times 10^{23} (site \cdot mol^{-1}) \times 0.6 \times 10^{-3} (g \cdot cm^{-2})}$$

$$= \frac{3.45\ (mA \cdot cm^{-2}) \times 10^{-3} (C \cdot s^{-1} \cdot mA^{-1})}{\frac{1.95 \times 10^{-2} (wt.\%)}{55.85 (g \cdot mol^{-1})} \times 6.02 \times 10^{23} (site \cdot mol^{-1}) \times 0.6 \times 10^{-3} (g \cdot cm^{-2})}$$

$$= \frac{3.45\ (mA \cdot cm^{-2}) \times 10^{-3} \times 6.25 \times 10^{18} (e^{-} \cdot s^{-1} \cdot mA^{-1})}{\frac{1.95 \times 10^{-2} (wt.\%)}{55.85 (g \cdot mol^{-1})} \times 6.02 \times 10^{23} (site \cdot mol^{-1}) \times 0.6 \times 10^{-3} (g \cdot cm^{-2})}$$

$$= 0.171\ (e^{-} \cdot site^{-1} \cdot s^{-1})$$

Where W_{Fe-N4} and M_{Fe} ($|M_{Fe}|$=55.85 g mol^{-1}) are the mass fraction and molar mass of Fe, respectively. W_{Fe-N4} ($W_{Fe-N4} = 1.95 \times 10^{-2}\ wt.\%$) is measured from ICP-MS analysis. j_k is the mass transfer corrected kinetic current density. N_A is Avogadro's number (6.02×10^{23} mol^{-1}).

For the NiFe&FeNCL/G catalyst, there are two active parts. One is the Fe-N_4 active sites and the other is Fe-N_4 moieties modified by the NiFe hydroxides. We hypothesized that NiFe hydroxide ($NiFe(OH)_x$) species are not contributed to the BET surface area in NiFe&FeNCL/G, the loading of NiFe hydroxides can be derived from the ICP-MS/BET data, showing $\varphi_{NiFe(OH)x} = \sim 18.5$ wt.% in NiFe&FeNCL/G (the FeNCL/G substrate is $\varphi_{FeNCL/G} = \frac{377.8}{463.4} = \sim 81.5$ wt.%). The Fe and Ni contents in the NiFe hydroxides of NiFe&FeNCL/G are 3.01 wt.% (4.60-1.95*0.815=~3.01) and 1.57 wt.%, respectively. That is, Fe:Ni is ~2:1 in the NiFe hydroxides of NiFe&FeNCL/G. Based on the above analysis, the numbers of Fe-N_4 moieties ($N_{Fe\text{-}N4}$) from FeNCL/G, and Fe (N_{Fe}) and Ni (N_{Ni}) atoms from NiFe hydroxides in the work electrode are calculated as the follow:

$$N_{Fe-N4} = \frac{W_{Fe-N4} \times \varphi_{FeNCL/G}}{M_{Fe}} \times N_A \times m_{loading} \times A$$

$$= \frac{1.95 \times 10^{-2} \times 0.815}{55.85(g \cdot mol^{-1})} \times 6.02 \times 10^{23}(site \cdot mol^{-1}) \times 0.6 \times 10^{-3}(g \cdot cm^{-2}) \times 10^{19}\ (site)$$

$$N_{Fe} = \frac{W_{Fe} - W_{Fe-N4} \times \varphi_{FeNCL/G}}{M_{Fe}} \times N_A \times m_{loading} \times A$$

$$= \frac{4.6 \times 10^{-2} - 1.95 \times 10^{-2} \times 0.815}{55.85(g \cdot mol^{-1})} \times 6.02 \times 10^{23}(site \cdot mol^{-1}) \times 0.6 \times cm^2) = 3.82 \times 10^{19}\ (site)$$

$$N_{Ni} = \frac{W_{Ni}}{M_{Ni}} \times N_A \times m_{loading} \times A$$

$$= \frac{1.57 \times 10^{-2}}{58.69(g \cdot mol^{-1})} \times 6.02 \times 10^{23}(site \cdot mol^{-1}) \times 0.6 \times 10^{-3}(g \cdot cm^{-2}) \times 10^{19}\ (site)$$

Where A is the area of work electrode, M_{Ni} ($|M_{Ni}|$=58.69 g mol^{-1}) are the mass fraction and molar mass of Fe, respectively. W_{Fe} (W_{Fe} = *4.6 wt.%*) and W_{Ni} (W_{Fe} = *1.57 wt.%*) are measured from ICP-MS analysis.

Since the average size of NiFe hydroxides of NiFe&FeNCL/G is ~2.1 nm, we hypothesized that NiFe hydroxides, belong to hexagonal crystal system, are single-layer species. Together with the bond length (0.284 nm) of Fe-Ni, Fe-Fe and/or Ni-Ni (*SusMat 2024, 4, e201*), one NiFe hydroxide nanoparticle (2.1 nm) contains the number of Fe/Ni atoms ($N_{Fe/Ni}$) as the follow:

$$N_{Fe/Ni} = \frac{3.14 \times (\frac{2.1}{2})^2}{\frac{3}{6} \times \frac{1}{2} \times \frac{\sqrt{3}}{2} \times (0.284)^2}$$

$$= 1.98 \times 10^2$$

Thus, the number of the NiFe hydroxide nanoparticles ($N_{NiFe(OH)x}$) in the electrode are calculated as the follow:

$$N_{NiFe(OH)x} = \frac{N_{Fe} + N_{Ni}}{N_{Fe/Ni}} = \frac{3.82 \times 10^{19} + 1.90 \times 10^{19}}{1.98 \times 10^2} = 2.89 \times 10^{17}(site)$$

We hypothesized that one NiFe (NiFe(OH)$_x$) modified one Fe-N$_4$ moiety. Thus, the TOF of NiFe hydroxide-modified Fe-N$_4$ moiety ($TOF_{NiFe/Fe\text{-}N4}$) is calculated from the follow:

$$I_k \approx TOF_{Fe-N4} \times (N_{Fe-N4} - N_{NiFe/Fe-N4}) + TOF_{NiFe/Fe-N4} \times N_{NiFe/Fe-N4}$$

$$= TOF_{Fe-N4} \times (N_{Fe-N4} - N_{NiFe(OH)x}) + TOF_{NiFe/Fe-N4} \times N_{NiFe(OH)x}$$

That is,

$$3.24(mA{\cdot}cm^{-2}) \times 0.19625(cm^2) = 3.24\,(mA{\cdot}cm^{-2}) \times 10^{-3}(A{\cdot}mA^{-1}) \times 0.19625(cm^2) = 3.24\,(mA{\cdot}cm^{-2}) \times 10^{-3}\,(C{\cdot}s^{-1}{\cdot}mA^{-1}) \times 0.19625(cm^2) = 3.24\,(mA{\cdot}cm^{-2}) \times 10^{-3} \times 6.25 \times 10^{18}(e^{-}{\cdot}s^{-1}{\cdot}mA^{-1}) \times 0.19625(cm^2) = 3.974 \times 10^{18}(e^{-}{\cdot}s^{-1}) = 0.171(e^{-}{\cdot}site^{-1}{\cdot}s^{-1}) \times (2.02 \times 10^{19} - 2.89 \times 10^{17})(site) + TOF_{NiFe/Fe-N4} \times 2.89 \times 10^{17}(site)$$

Thus, $TOF_{NiFe/Fe-N4} = 1.97\ (e^{-}{\cdot}site^{-1}{\cdot}s^{-1})$

4. ZAB tests

ZABs were assembled in homemade cells. Catalyst ink was loaded on a porous carbon paper as the air electrode. The catalyst loading was 0.8 mg cm^{-2}. A Zn plate was used as the anode. A 6 M KOH aqueous solution with 0.2 M zinc acetate was used as the electrolyte. Polarization curve measurements of ZABs were performed on an electrochemical analysis station (CHI 700 E, 760 E and 1130 E, CH Instruments, China). Galvanostatic charge-discharge cycling measurements of ZABs were carried out on battery testing system (CT-4008, NEWARE, China).

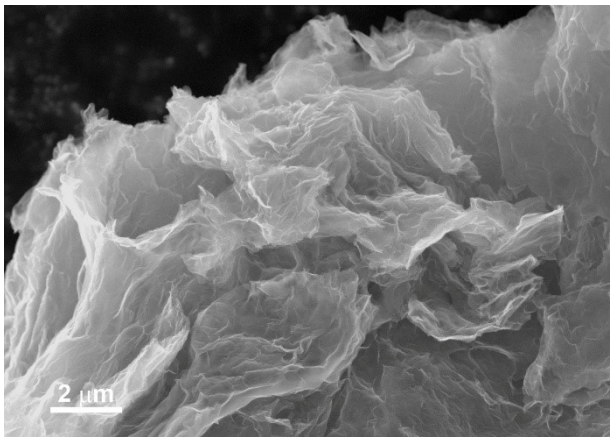

Figure S1. SEM image of G.

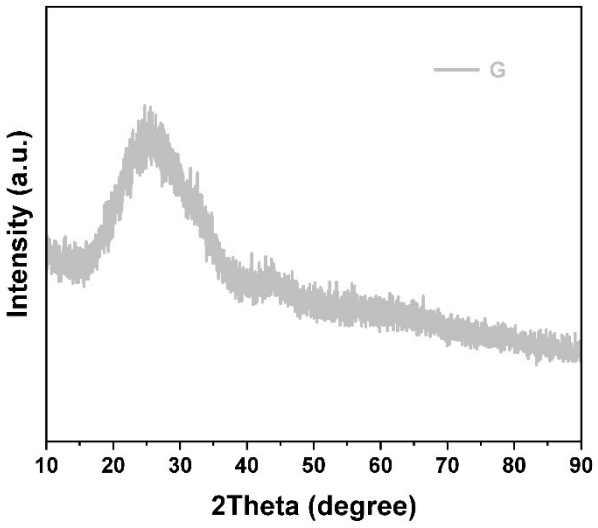

Figure S2. XRD pattern of G.

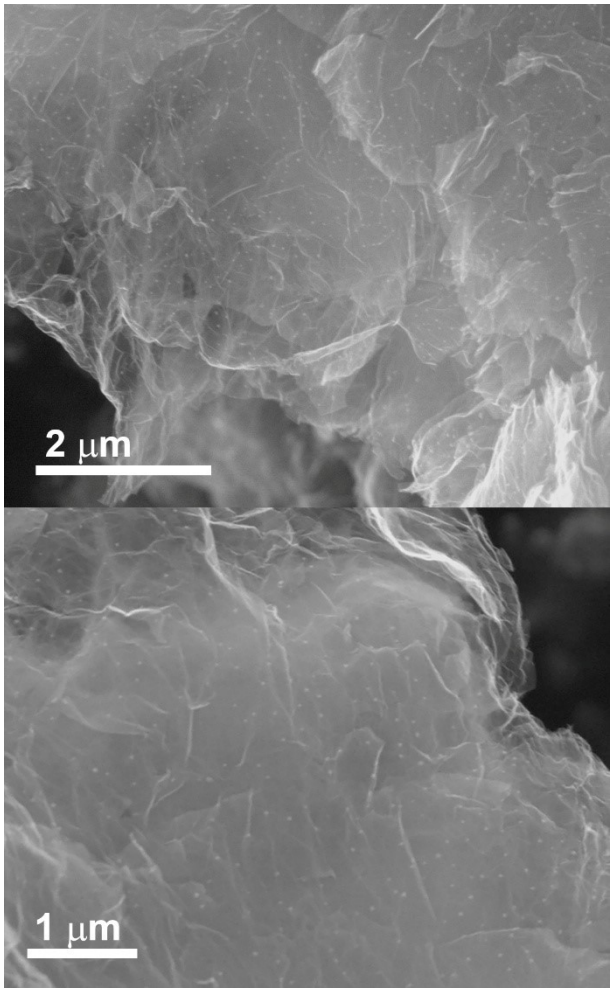

Figure S3. SEM images of Fe-ZIF/G.

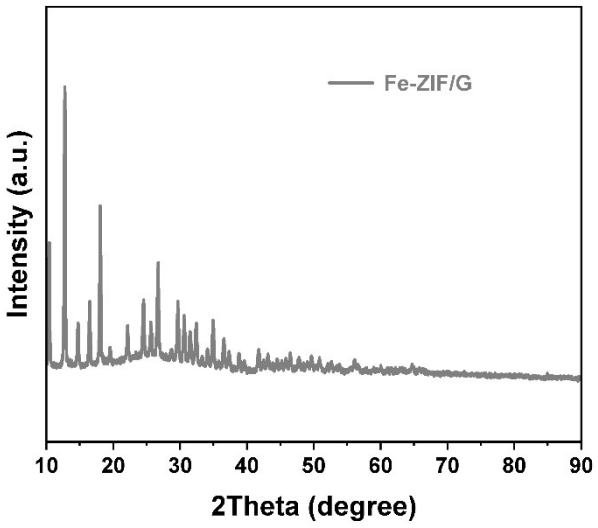

Figure S4. XRD pattern of Fe-ZIF/G.

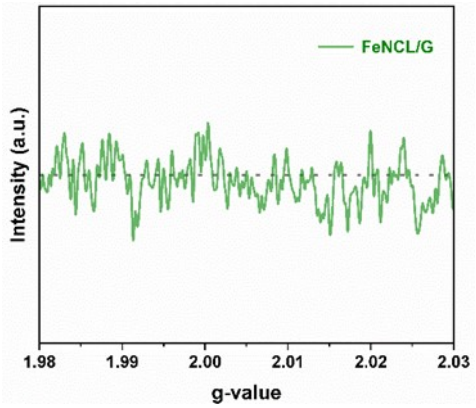

Figure S5. EPR spectrum of FeNCL/G.

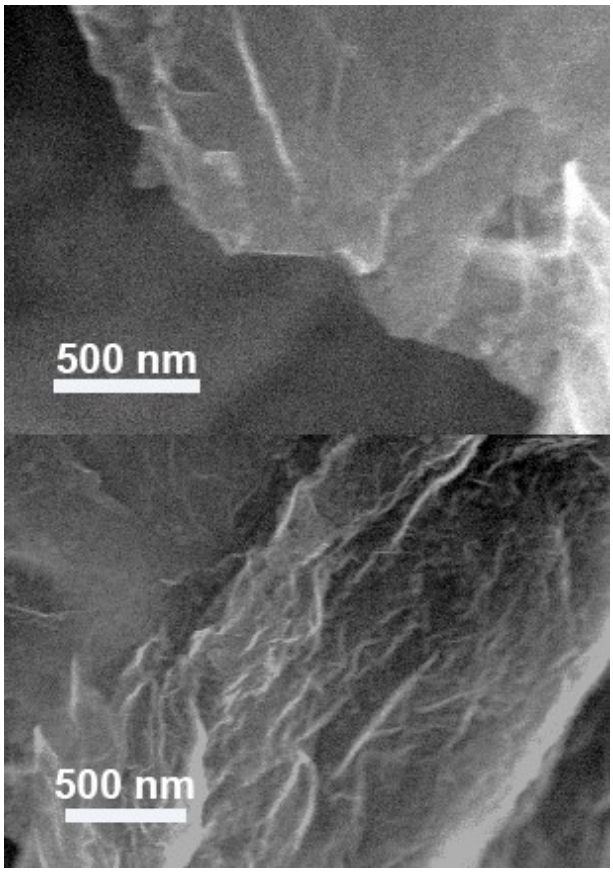

Figure S6. SEM images of FeNCL/G.

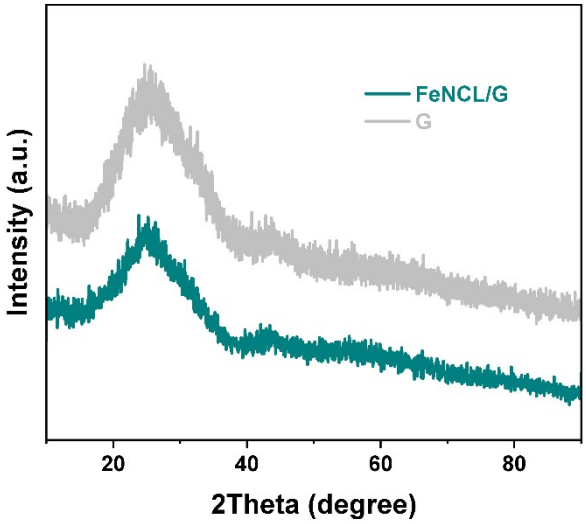

Figure S7. XRD pattern of FeNCL/G.

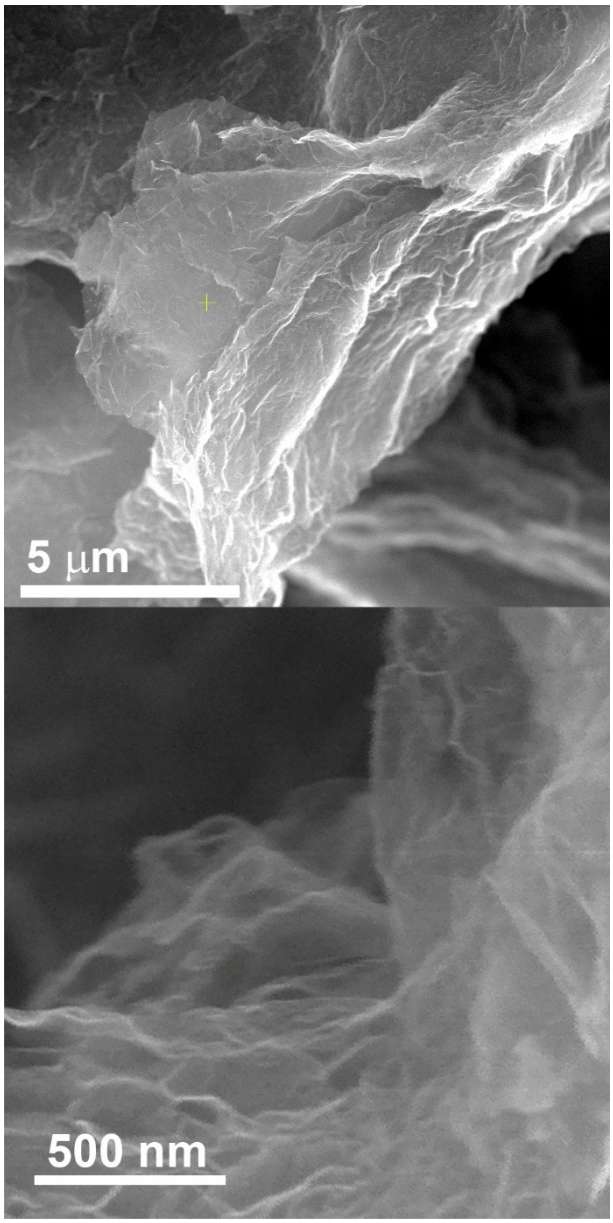

Figure S8. SEM images of NiFe&FeNCL/G.

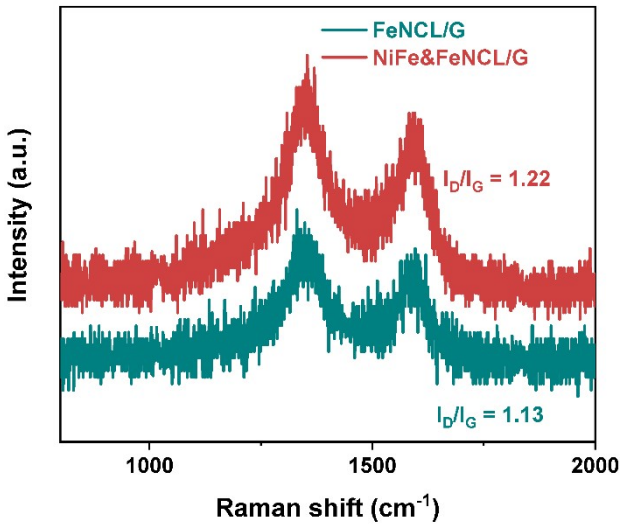

Figure S9. Raman spectra of NiFe&FeNCL/G and FeNCL/G.

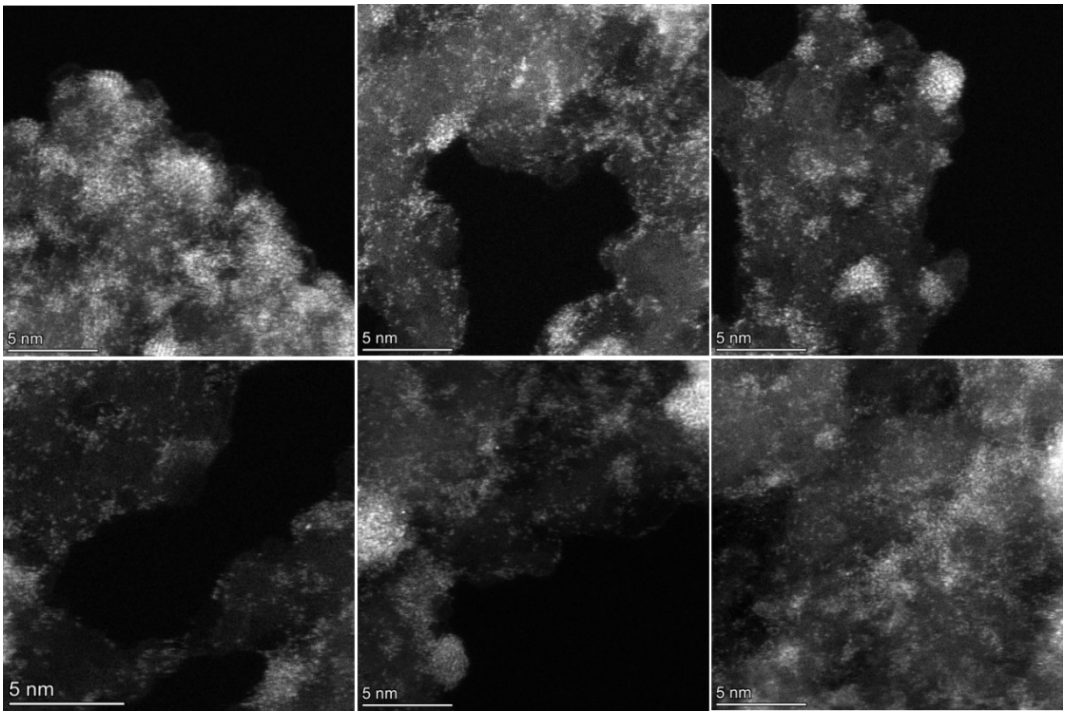

Figure S10. STEM images of NiFe&FeNCL/G.

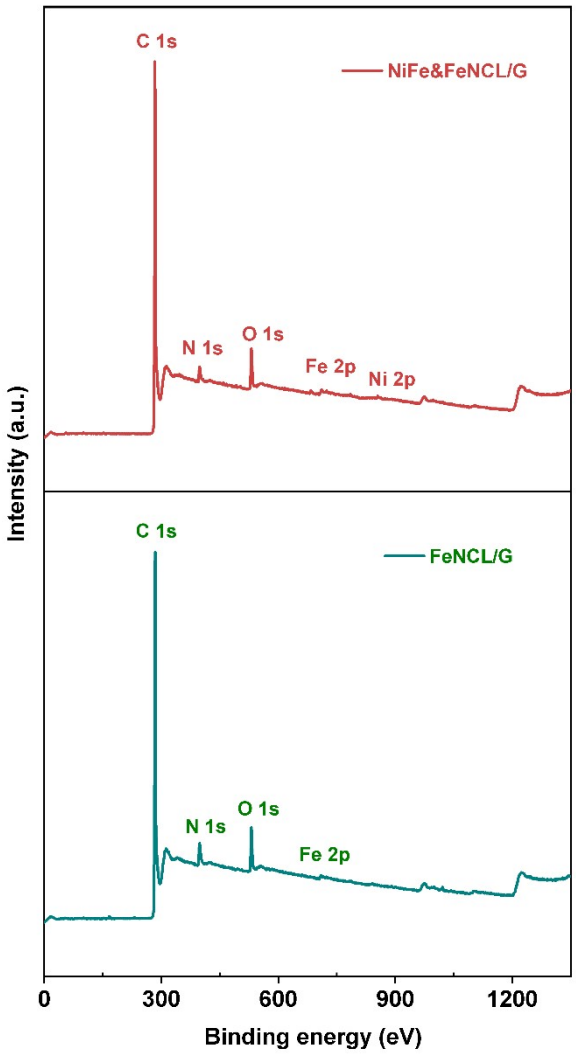

Figure S11. XPS spectra of NiFe&FeNCL/G and FeNCL/G.

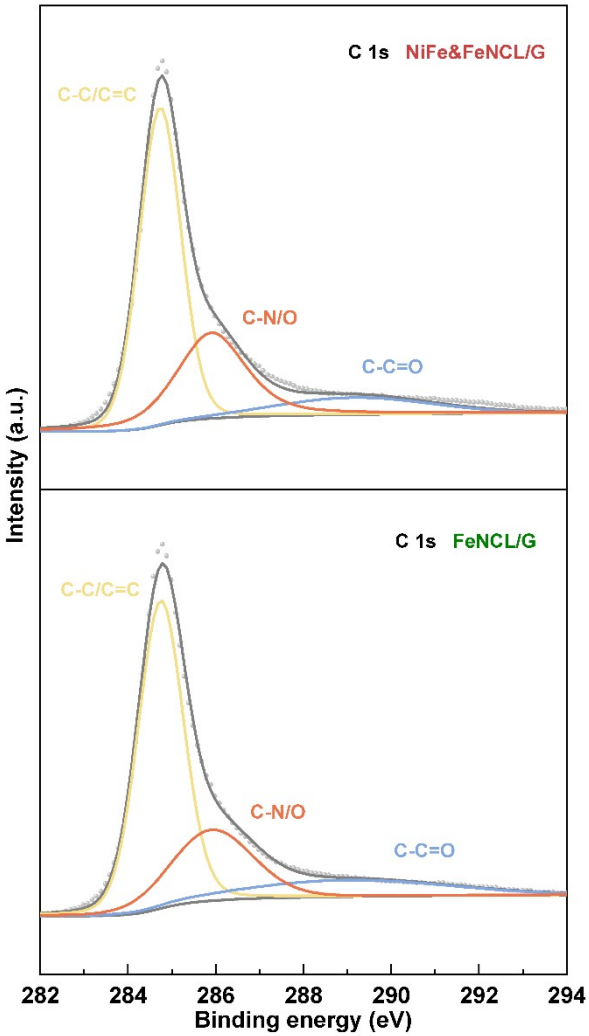

Figure S12. C 1s XPS spectra of NiFe&FeNCL/G and FeNCL/G.

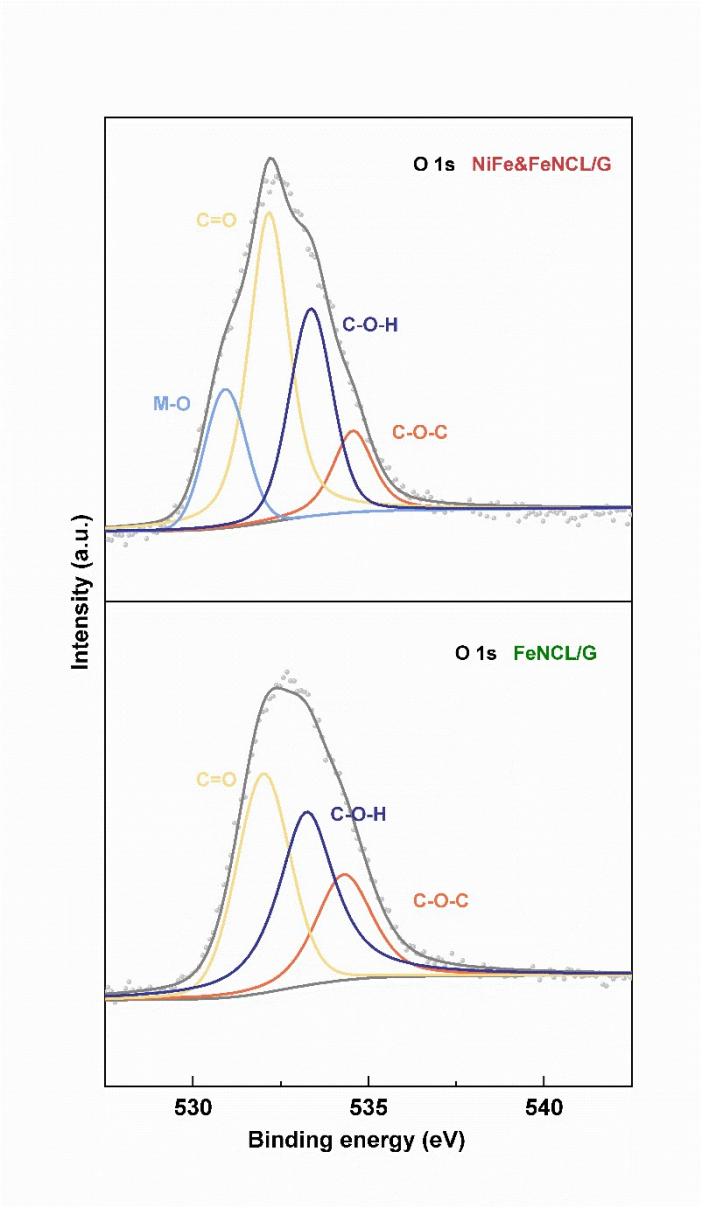

Figure S13. O 1s XPS spectra of NiFe&FeNCL/G and FeNCL/G.

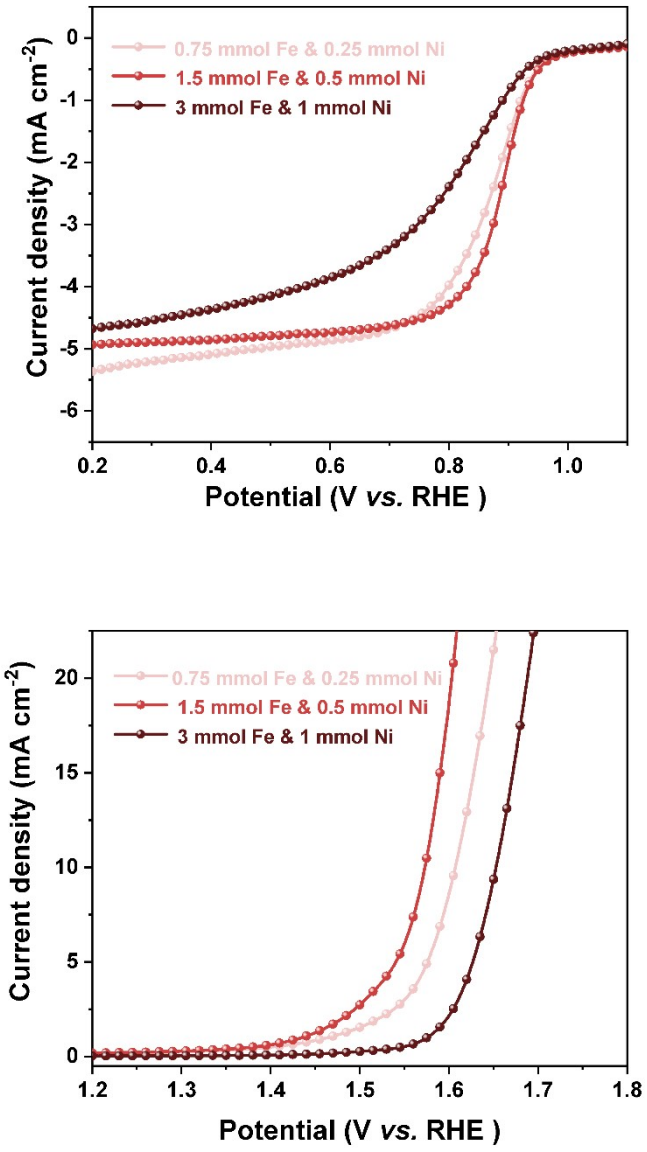

Figure S14. ORR and OER polarization curves of the samples prepared with different contents of Fe (from $Fe(NO_3)_3 \cdot 9H_2O$) and Ni (from $Ni(NO_3)_2 \cdot 6H_2O$).

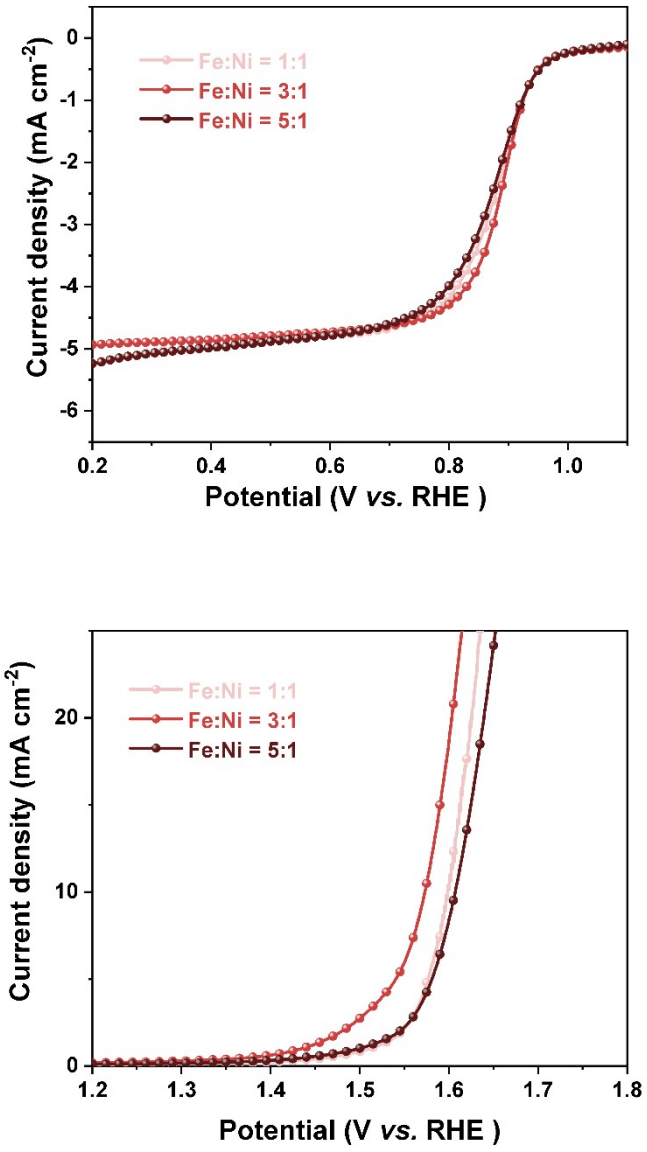

Figure S15. ORR and OER polarization curves of the samples prepared with different proportions of Fe (from $Fe(NO_3)_3 \cdot 9H_2O$) and Ni (from $Ni(NO_3)_2 \cdot 6H_2O$).

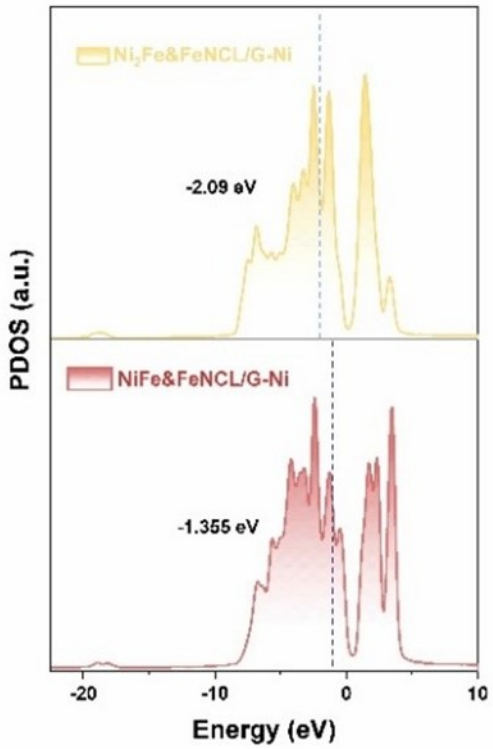

Figure S16. PDOS plots showing the d-band centers of NiFe&FeNCL/G (Fe:Ni=2:1), Ni_2Fe&FeNCL/G (Fe:Ni=1:2) and NiFeLDH (Fe:Ni=2:1, the absence of FeNCL/G).

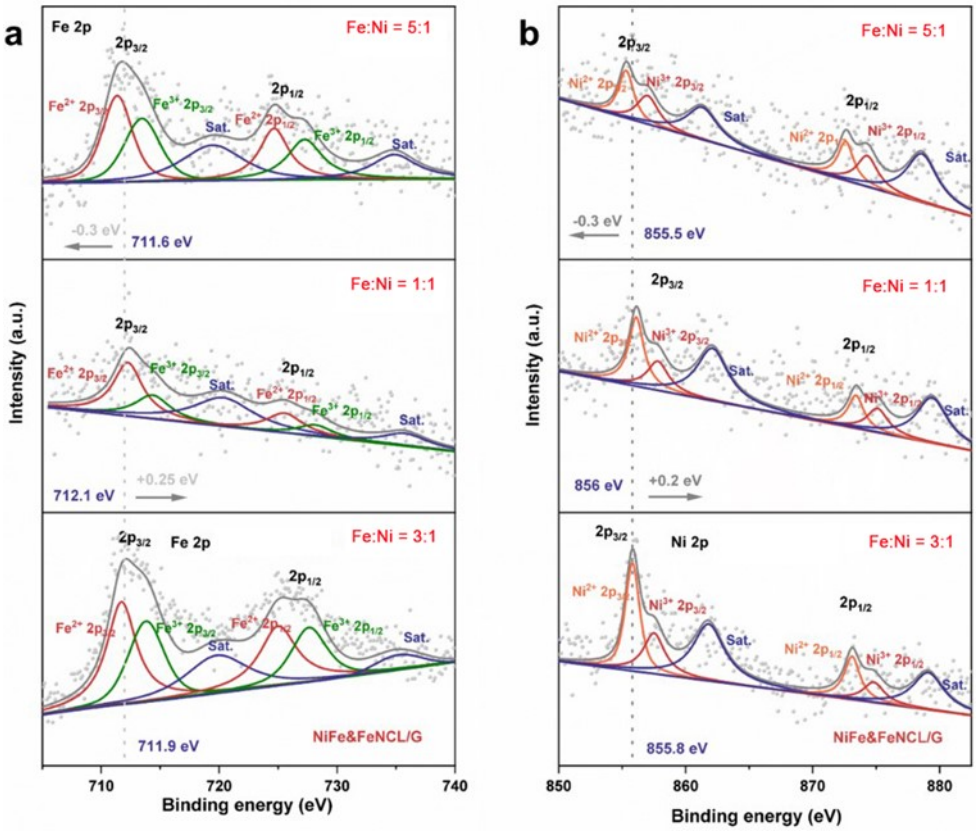

Figure S17. (a) Fe 2p and (b) Ni 2p XPS spectra of the samples prepared with different ratios of Fe (from $Fe(NO_3)_3 \cdot 9H_2O$) and Ni (from $Ni(NO_3)_2 \cdot 6H_2O$).

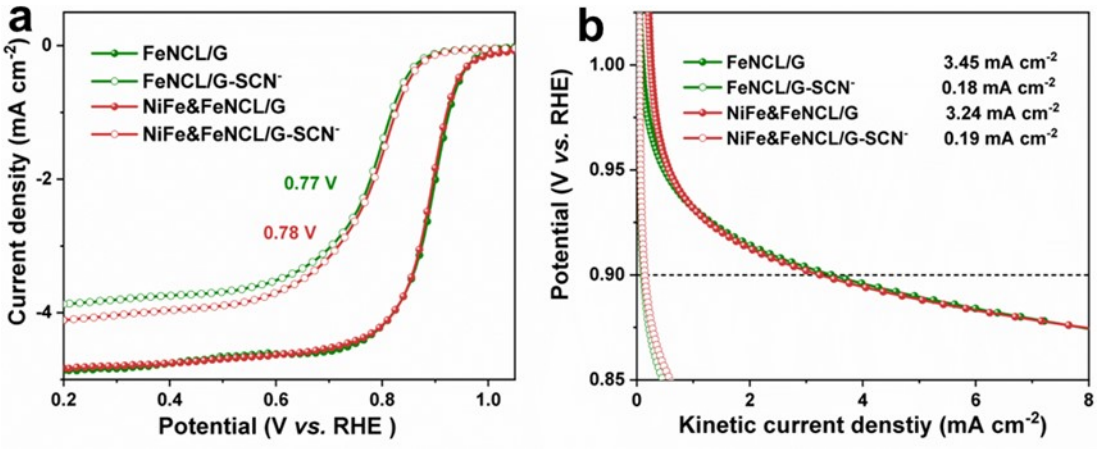

Figure S18. (a) ORR polarization curves and (b) kinetic current density curves of NiFe&FeNCL/G and FeNCL/G before and after poisoning.

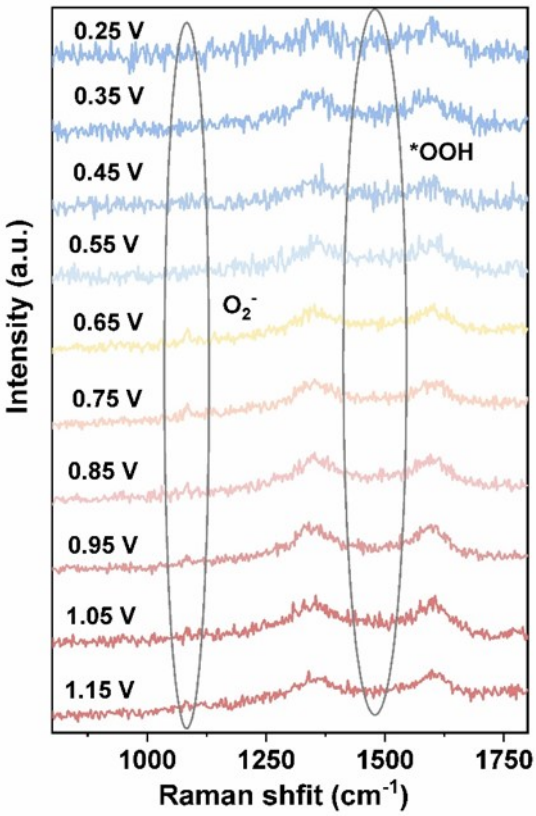

Figure S19. *In-situ* Raman spectra of NiFe&FeNCL/G during the ORR process

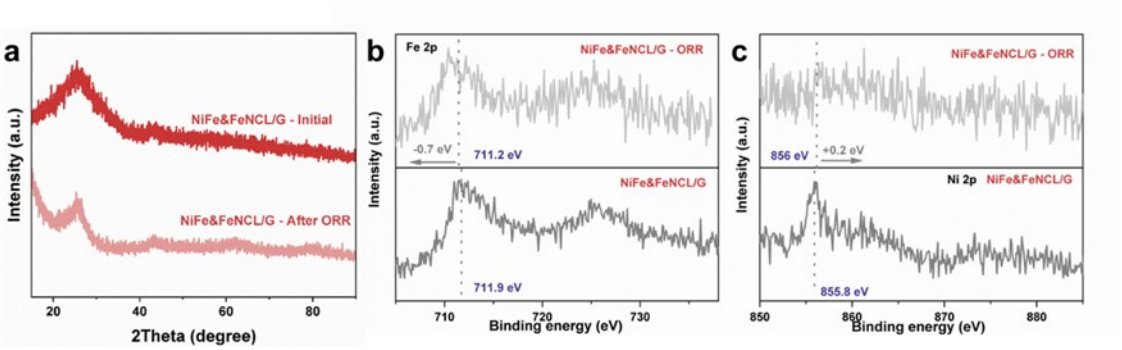

Figure S20. (a) XRD patterns, (b) Fe 2p and (c) Ni 2p XPS spectra of NiFe&FeNCL/G before and after the ORR durability tests.

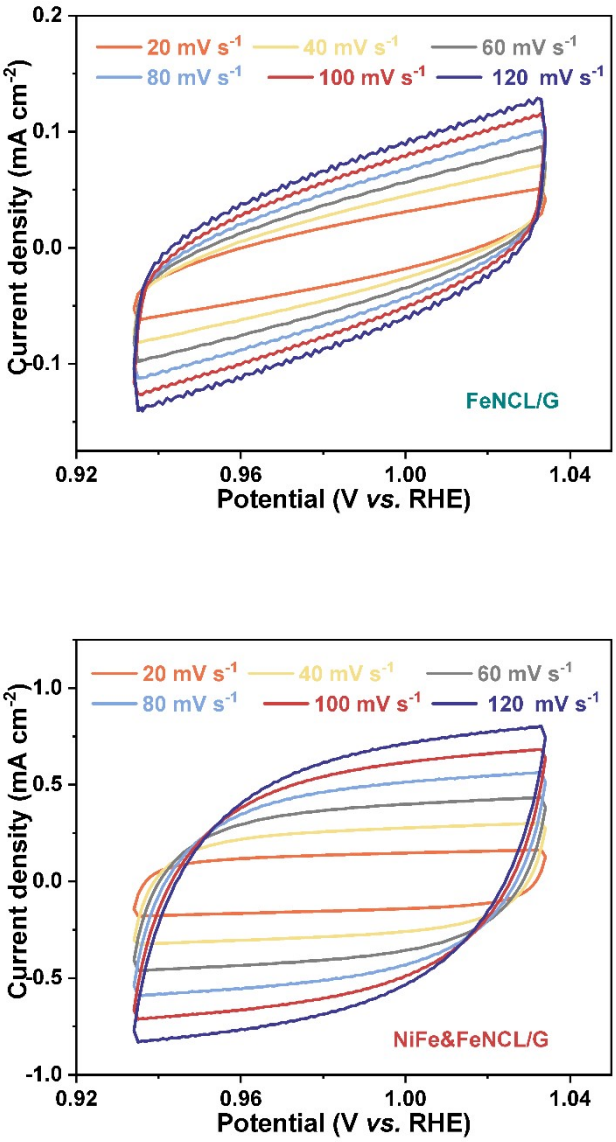

Figure S21. CV curves of NiFe&FeNCL/G and FeNCL/G recorded at different scan rates.

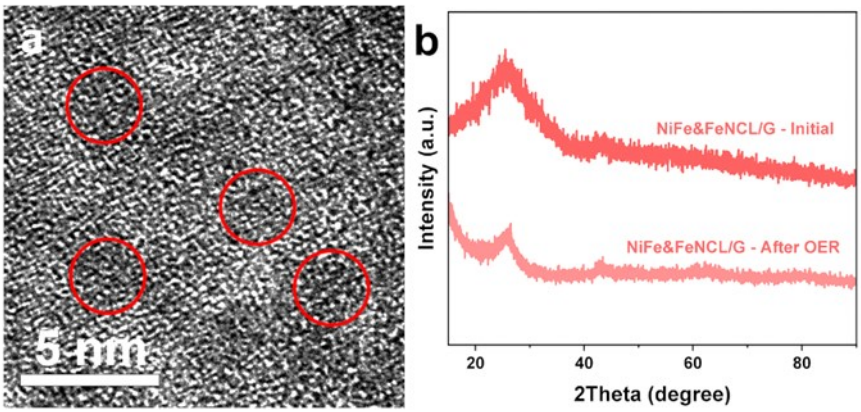

Figure S22. (a) TEM image of NiFe&FeNCL/G after the OER durability test. (b) XRD patterns of NiFe&FeNCL/G before and after ORR durability tests.

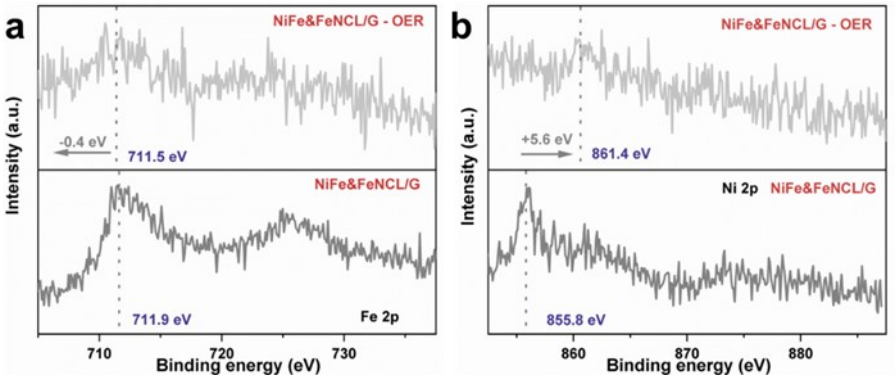

Figure S23. (a) Fe 2p and (b) Ni 2p XPS spectra of NiFe&FeNCL/G before and after ORR durability tests.

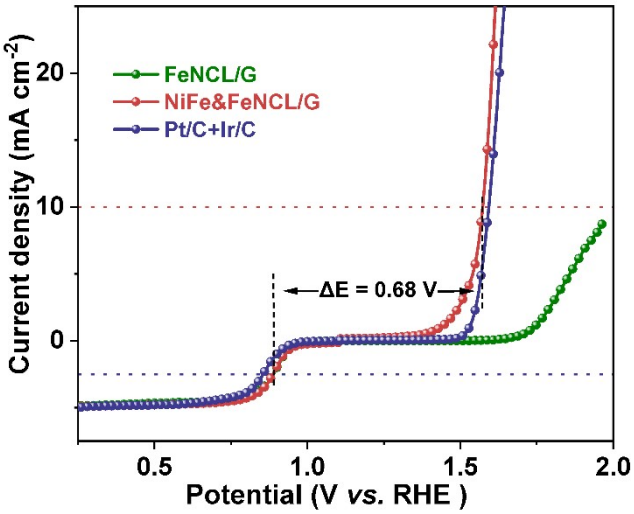

Figure S24. Oxygen electrocatalytic performances of NiFe&FeNCL/G, FeNCL/G, and Pt/C+Ir/C.

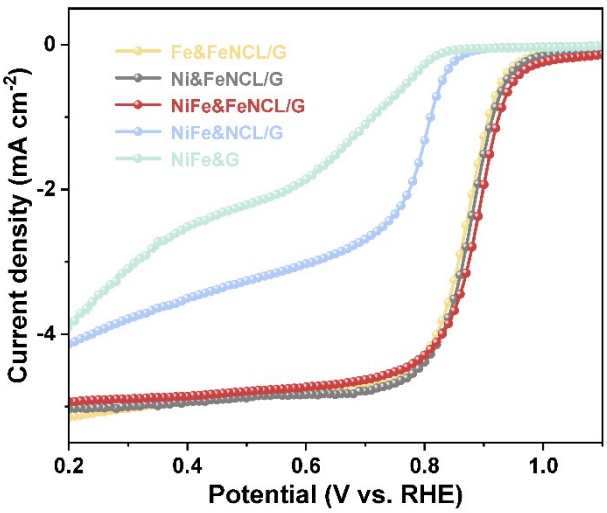

Figure S25. ORR polarization curves of NiFe&FeNCL/G, Ni&FeNCL/G, Fe&FeNCL/G, NiFe&NCL/G and NiFe&G.

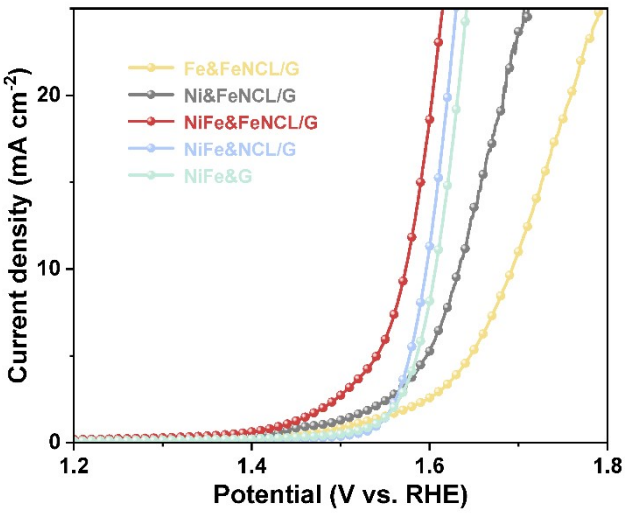

Figure S26. OER polarization curves of NiFe&FeNCL/G, Ni&FeNCL/G, Fe&FeNCL/G, NiFe&NCL/G and NiFe&G.

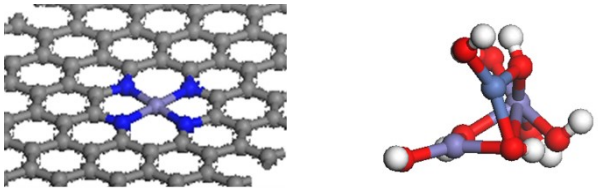

Figure S27. Optimized stable structures of FeNCL/G (left) and NiFe hydroxide (right).

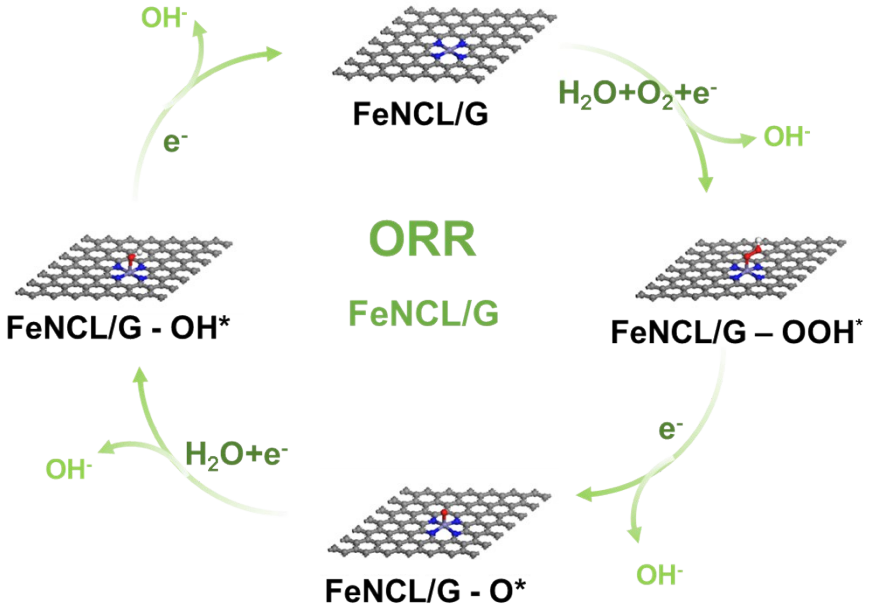

Figure S28. Absorbate evolution mechanism for ORR on active site of FeNCL/G.

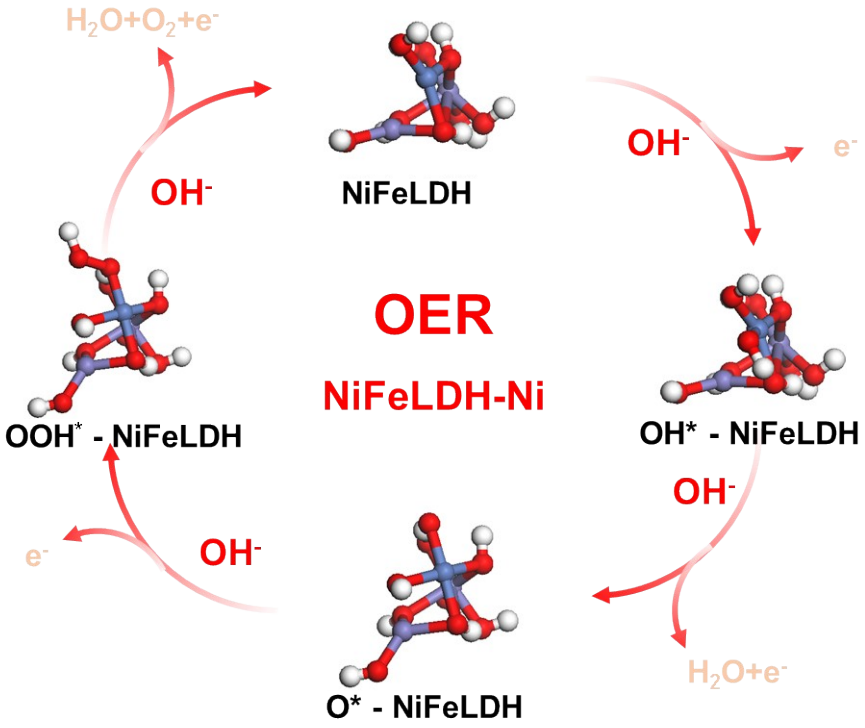

Figure S29. Absorbate evolution mechanism for OER on active site of NiFe hydroxide.

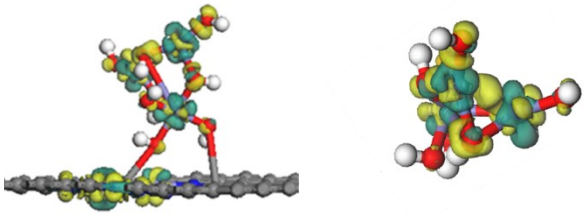

Figure 30. Charge density differences of NiFe&FeNCL/G and NiFe hydroxide.

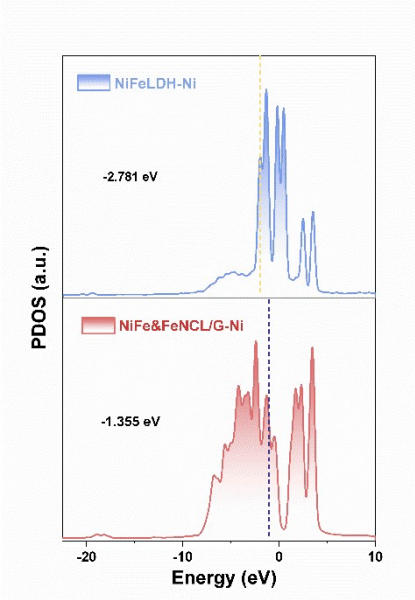

Figure S31. Projected density of states (PDOS) of Ni active centers in NiFeLDH and NiFe&FeNCL/G.

Table R1. A performance comparison of NiFe&FeNCL/G and other NiFe/Fe-N_4 catalysts.

Sample	ORR	OER	ΔE	Reference
FePc||$NiFe_2O_4$/G	0.85 V	1.57 V	0.72 V	*Energy Storage Mater.* ***2023****, 54, 517-523*
Ni_3Fe@CNTs/Fe-N_4	0.86 V	1.59 V	0.73 V	*Appl. Catal. B Environ.* ***2024,*** *354, 124151*
NiFe-LDH/Fe_1-N-C	0.9 V	1.56 V	0.66 V	*Adv. Energy Mater.* ***2023,*** *13, 2203609*
NiFe-LDH/Fe,N-CB	0.84 V	1.50 V	0.71 V	*ACS Appl. Mater. Interfaces* ***2023,*** *15, 16732–16743*
LDH/FeNCF	0.85 V	1.55 V	0.70 V	*J. Energy Storage, 2023, 72, 108073*
$Ni_{66}Fe_{34}$-NC	0.85 V	1.69 V	0.84 V	*Appl. Catal. B Environ.* ***2020,*** *274, 119091*
NiFe–N–C	0.87 V	1.55 V	0.68 V	*Energy Environ. Sci. 2024, 17, 704-716*
Pt/C+Ir/C	**0.84 V**	**1.59 V**	**0.75 V**	**This work**
NiFe&FeNCL/G	**0.89 V**	**1.57 V**	**0.68 V**	**This work**

Table R2. A liquid-state ZAB performance comparison of NiFe&FeNCL/G and other NiFe/Fe-N_4 catalysts.

Sample	Power density (mW cm^{-2})	Specific capacities (mAh g^{-1})	Reference
FePc||$NiFe_2O_4$/G	185	741	*Energy Storage Mater.* ***2023****, 54, 517-523*
NF@GF/rGO-FePc||FeNi	220.2	739.3	*SusMat.* ***2024****,4, e201*
NiFe-LDH/Fe_1-N-C	205	815	*Adv. Energy Mater.* ***2023,*** *13, 2203609*
FeNi SAs/NC	/	779.4	*Adv. Energy Mater.* ***2021,*** *11, 2101242*
$Ni_{66}Fe_{34}$-NC	223	798.2	*Appl. Catal. B Environ.* ***2020,*** *274, 119091*
Ni_3Fe@CNTs/Fe-N_4	150	797.4	*Appl. Catal. B Environ.* ***2024,*** *354, 124151*
FeNi/CNT-FePc	208	751.1	*Inorg. Chem. Front.* ***2025,*** *12, 4409*
Pt/C+Ir/C	**185.5** **329.9 (O_2)**	**708.0**	**This work**
NiFe&FeNCL/G	**242.2** **404.9 (O_2)**	**798.8**	**This work**

Table R3. DOD and RTE of liquid-state ZABs.

Sample	DOD	RTE (@time)		
Pt/C+Ir/C	**78.1%**	**62.9% (@0 h)**	**58.3% (@25 h)**	**54.6% (@50 h)**
NiFe&FeNCL/G	**95.4%**	**65.3% (@0 h)**	**65.3% (@350 h)**	**65.3% (@700 h)**

Table R4. RTE of solid-state ZABs.

Sample	RTE		
Pt/C+Ir/C	**48.3% (@0 h)**	**44.0% (@12 h)**	**43.2% (@24 h)**
NiFe&FeNCL/G	**63.3% (@0 h)**	**62.7% (@36 h)**	**62.2% (@72 h)**

Table S5. A solid -state ZAB performance comparison of ZAB electrocatalysts.

Sample	Power density (mW cm^{-2})	Stability test	Reference
FePc||$NiFe_2O_4$/G	66	8 h @2 mA cm^{-2}	*Energy Storage. Mater.* ***2023**, 54, 517-523*
NF@GF/rGO-FePc||FeN	77.6	24 h@2mA cm^{-2}	*SusMat.* ***2024**,4, e201*
FeNP||FeSA/NHTPC-Co	110 (O_2)	72 h@2 mA cm^{-2}	*J. Colloid Interface Sci.* ***2024**, 664,1012–1020*
Pt/C+Ir/C	**91.6** **106.1 (O_2)**	**/**	**This work**
NiFe&FeNCL/G	**103.8** **129.2 (O_2)**	**72 h@2mA cm^{-2}**	**This work**